Research Square

Preprints are preliminary reports that have not undergone peer review.
They should not be considered conclusive, used to inform clinical practice,
or referenced by the media as validated information.

Organization of ice multiplication mechanisms among basic cloud types. Part I: control simulations

Akash Deshmukh

akash.deshmukh@univ-lille.fr

Université de Lille

Deepak Waman

Lund University

Ashok Kumar Gupta

Vanderbilt University

Martanda Gautam

Lund University

Vaughan Phillips

Lund University

Aaron Bansemer

NSF National Center for Atmospheric Research

Paul Connolly

University of Manchester

Greg McFarquhar

University of Oklahoma

Paul DeMott

Colorado State University

Jiwen Fan

Argonne National Laboratory

Yun Lin

University of California, Los Angeles

Jann Schrod

Goethe University Frankfurt

Heinz Bingemer

Goethe University Frankfurt

Article

Keywords:

Posted Date: November 18th, 2026

DOI: https://doi.org/10.21203/rs.3.rs-11639712/v1

License: This work is licensed under a Creative Commons Attribution 4.0 International License.
Read Full License

Additional Declarations: No competing interests reported.

Organization of ice multiplication mechanisms among basic cloud types. Part I: control simulations

Akash Deshmukh[1,2*], Deepak Waman[1,3], Ashok Kumar Gupta[4], Martanda Gautam[1,5], Vaughan Phillips[1*], Aaron Bansemer[6], Paul Connolly[7], Greg McFarquhar[8], Paul J. DeMott[9], Jiwen Fan[10], Yun Lin[11], Jann Schrod[12], Heinz Bingemer[12]

[1]Department of Physical Geography and Ecosystem Science, University of Lund, Lund, Sweden.
[2]University of Lille, CNRS, UMR 8518 - LOA - Laboratoire d'Optique Atmospherique, Lille, France.
[3]Currently at Institute of Meteorology and Climate Research Troposphere Research, Karlsruhe Institute of Technology, Karlsruhe, Germany, Karlsruhe, Germany.
[4]Department of Earth and Environmental Sciences, Vanderbilt University, Nashville, Tennessee, USA.
[5]Currently at Johannes Gutenberg University, Mainz, Germany.
[6]Mesoscale and Microscale Meteorology Laboratory, National Center for Atmospheric Research, Boulder, Colorado, USA.
[7]Department of Earth and Environmental Sciences and Cooperative Institute for Severe and High Impact Weather Research and Operations, The University of Manchester, Manchester, UK.
[8]School of Meteorology and Cooperative Institute for Severe and High Impact Weather Research and Operations, University of Oklahoma, Norman, OK, USA.
[9]Department of Atmospheric Science, Colorado State University, CO, USA.
[10]Environmental Science Division, Argonne National Laboratory, IL, USA.
[11]Joint Institute for Regional Earth System Science and Engineering, University of California, Los Angeles, Los Angeles, CA, USA.
[12]Institute for Atmospheric and Environmental Sciences, Goethe-University, Frankfurt, Germany.

*Corresponding author(s). E-mail(s): akash.deshmukh@univ-lille.fr; vaughan.phillips@mgeo.lu.se;

Abstract

Observed ice particle concentrations frequently exceed those expected from primary ice nucleation, highlighting the importance of Secondary ice production (SIP). Though, the relative importance of individual SIP mechanisms remain poorly understood across diverse clouds. We quantify the contributions of four SIP mechanisms in convective and stratiform clouds with cloud-base temperatures of $\mathbf{0°C}$ (cold-based convective clouds), $\mathbf{17°C}$ (warm-based), and $\mathbf{25°C}$ (very-warm based) using a cloud-resolving Aerosol–Cloud model. We find that ice–ice collisional breakup is the dominant SIP mechanism over the simulated cloud life cycles, whereas the Hallett–Mossop (HM) process becomes particularly important under specific thermodynamic and dynamical conditions. In warm-based convection, increasing vertical velocity from $\mathbf{2}$ to $\mathbf{20}\ \boldsymbol{ms^{-1}}$ increases the predicted HM-related ice enhancement ratio from $\mathbf{10^2}$ to $\mathbf{10^3}$ within the $\mathbf{0}$ and $\mathbf{-15°C}$. Breakup in ice–ice collisions dominates secondary ice production in all four cloud types, and sublimational breakup ranks second even after discounting fragments that sublimate completely; models representing secondary ice solely through the HM process omit both. Cloud-base temperature governs which mechanisms are active and vertical velocity where they operate.

Keywords: cloud, secondary ice, microphysics, stratiform

1 Introduction

Why ice particle concentrations in clouds often far exceed those expected from primary ice nucleation remains a longstanding question in cloud physics [1–7]. Secondary ice production (SIP) offers an explanation, generating new ice particles from those already present through several proposed mechanisms: the Hallett–Mossop (HM) rime-splintering process [8], raindrop-freezing fragmentation [9, 10], ice–ice collisional breakup [11–13], and fragmentation during ice sublimation [14–17]. Each requires different conditions of temperature, supercooled liquid water and hydrometeor population, yet their relative importance across cloud types remains poorly constrained by observationally-constrained cloud resolving models. Meanwhile the HM process remains the most frequently implemented, and often the only, SIP mechanism in weather and climate models [4], although its efficiency has recently been questioned in the laboratory [18]. Which mechanism prevails in which cloud is therefore an open question, and the answer should depend on how each cloud forms its precipitation.

SIP could fragment precipitation hydrometeors, whether supercooled drops or ice, so the extent of ice multiplication depends on the microphysical conditions at subfreezing temperatures that govern how those hydrometeors grow. A deep cloud can have one, or both, of two sets of mechanisms for precipitation production [19]:

- The '*warm rain process*' involving coalescence of cloud-droplets if large enough, which can happen in principle at any temperature where liquid is present, and which aloft can yield supercooled drizzle or rain that freezes ('warm' graupel);
- The '*ice crystal process*' involving vapor growth of crystals to form snow that may grow by aggregation of crystals or may fall out, perhaps melting as 'cold' rain/drizzle or may rime to form 'cold' graupel that then falls out.

Figure 1 maps both pathways (red and blue) and their links to SIP. The terms 'warm' and 'cold' denote the mechanism, not the ambient temperature; the ice crystal process requires mixed-phase conditions, with INPs active at temperatures warmer than $-40\,^{\circ}\mathrm{C}$ [20] and humidity near water saturation for fast vapor growth. Which pathway prevails in a cloud should therefore decide which SIP mechanisms prevail with it.

In mixed-phase clouds that balance is set by cloud-base temperature and aerosol conditions [21, 22], which together control the mean cloud-droplet diameter aloft; coalescence requires droplets of at least about $20\,\mu\mathrm{m}$ [19, 23]. In convective clouds with a cold base (colder than about $10\,^{\circ}\mathrm{C}$), where the ice crystal process prevails without coalescence, simulations show SIP driven mostly by fragmentation in ice–ice collisions between graupel and snow, prolific from $0\,^{\circ}\mathrm{C}$ down to $-30\,^{\circ}\mathrm{C}$ or colder [24–28]; the droplets are too small to coalesce or to rime-splinter, and even where the HM process and raindrop freezing are active, as in the Midlatitude Continental Convective Clouds Experiment (MC3E), collisional breakup prevails over the cloud life cycle [27]. In deep convection with very warm bases, by contrast, the warm rain process dominates, so the HM process (droplets larger than about $24\,\mu\mathrm{m}$ between -3 and $-8\,^{\circ}\mathrm{C}$) and raindrop-freezing fragmentation can influence ice initiation [21], and 'warm' graupel from freezing rain colliding with secondary ice accelerates the multiplication [10]. Aerosols act through the same control: high CCN concentrations that suppress the warm rain process [19] curb 'warm' graupel and hence its rime-splintering or sublimational breakup [17], although ice multiplication can be so overwhelming as to damp this aerosol dependency [29]. Cloud-base temperature and aerosols thus decide which mechanisms are available; vertical motion decides where, and for how long, they act.

Updrafts loft supercooled raindrops and primary ice into the layers where the HM process and raindrop freezing operate, and faster updrafts balance precipitation particles aloft at larger sizes, allowing greater accretion rates and more energetic ice–ice collisions. Graupel and hail form mostly in convective ascent ($> 1\ \mathrm{m\ s^{-1}}$), large dense hail only in vigorous deep convection, whereas snow forms in weak stratiform ascent ($< 1\ \mathrm{m\ s^{-1}}$) [30]; in cold-based stratiform clouds the limited supercooled liquid weakens any SIP process that accretes it. Sublimational breakup instead requires ice-subsaturated air and is expected in downdrafts [17]. Vertical motion also sets lifetime, since clouds with weaker ascent tend to be longer lived [30], and this matters because the mechanisms differ in timescale: the fast HM process, peaking near $-5\,^{\circ}\mathrm{C}$, acts first in young clouds [31], and slower mechanisms supplement it later in deep convection [13, 26]. Convection lasting an hour or so may never let the slower processes become appreciably active, whereas stratiform cloud lasting many hours may.

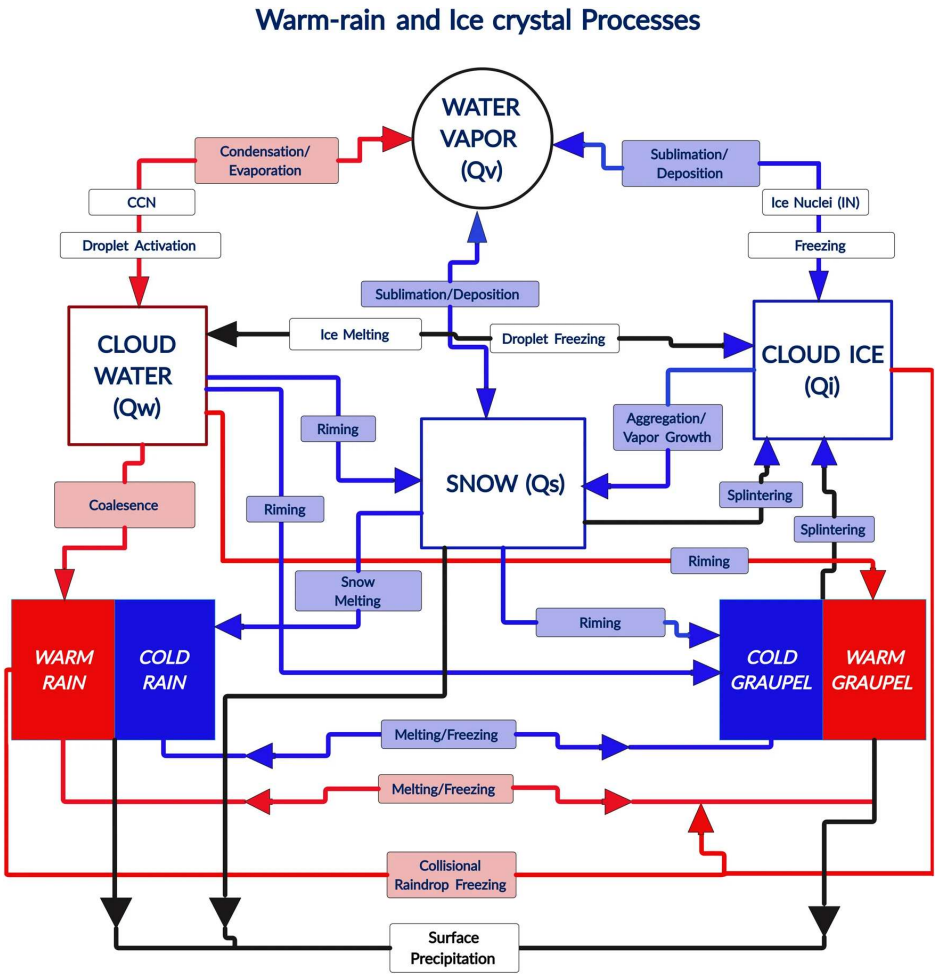


Fig. 1 Simplified map of microphysical conversions in clouds generally. Red arrows trace the warm-rain process, blue arrows trace the ice-crystal process, and black arrows mark transitions belonging to either pathway. Some SIP mechanisms are marked ('splintering'). Adapted from Gupta et al.[21].

The physical arguments above, based on droplet size, cloud-base temperature, aerosol loading, updraft and downdraft strength, and cloud lifetime, indicate where each SIP mechanism might be favored but not how much ice it produces in a given cloud. Answering that requires fragment production rates for each mechanism, and the laboratory and field data that constrain those rates differ greatly from one mechanism to the next. The raindrop-freezing fragmentation is relatively well established [10], whereas its 'Mode 2' (fragmentation when supercooled raindrops collide with ice) and sublimational breakup rely on limited evidence [17, 32]; ice–ice collisional breakup has been documented for natural and artificial snow [11, 33, 34], and the HM process is supported by aircraft observations [35, 36] but questioned in the laboratory [18]. Observations alone cannot settle the question, because a sampled ice particle carries no record of the mechanism that produced it. Numerical modeling validated against coincident field observations can attribute simulated ice to each mechanism and expose its dependence on cloud microphysical and environmental conditions [21, 37], which motivates a systematic, model-based examination of how the mechanisms are organized among basic cloud types.

The overall aim of this two-part study is to investigate how basic cloud types organize the relative activity of the SIP mechanisms. We define four 'basic cloud types', warm- and cold-based convective and stratiform clouds (Table 1), classifying cloudy grid points as convective or stratiform by $|w| > 1\,\mathrm{m\,s^{-1}}$ or $|w| < 1\,\mathrm{m\,s^{-1}}$ [38–40]. Four observed cases from the ACAPEX, STEPS, MC3E and GOAmazon campaigns are simulated with the aerosol conditions measured in each: stratiform cloud with a slightly cold base and convective clouds with cold, warm and very warm bases, whose stratiform regions provide the warm-based stratiform type. Each SIP mechanism is tagged with a tracer so that every ice particle can be attributed to its source, and the mechanisms are ranked by the simulation-averaged concentration of ice attributed to each. The questions are how updraft speed and cloud-base temperature regulate the influence of each mechanism, and how that influence depends on the INP and CCN activity of the aerosol.

Part I examines the relative activity of the SIP mechanisms in the control simulations of each cloud type, asking what role each process plays in the contrasting cloud types. Part II uses sensitivity simulations to ask the complementary causative question: what is the effect of each SIP process on the contrasting cloud types, and how would the clouds differ in its absence? Within the range of conditions and the empirically parameterized mechanisms considered here, we find that breakup in ice–ice collisions prevails in all four cloud types, that sublimational breakup, rather than the HM process, ranks second because fragments formed in downdrafts are mixed into adjacent ascent, and that cloud-base temperature and vertical velocity together organize the four mechanisms into a compact map.

Table 1 Basic classification of clouds (w is vertical velocity and T_b is cloud-base temperature).

	Warm-based		**Cold-based**	
Convective	$\lvert w\rvert > 1\ \mathrm{m\,s^{-1}}$,	$T_b >\sim 10°\mathrm{C}$	$\lvert w\rvert > 1\ \mathrm{m\,s^{-1}}$,	$T_b <\sim 10°\mathrm{C}$
Stratiform	$\lvert w\rvert < 1\ \mathrm{m\,s^{-1}}$,	$T_b >\sim 10°\mathrm{C}$	$\lvert w\rvert < 1\ \mathrm{m\,s^{-1}}$,	$T_b <\sim 10°\mathrm{C}$

2 Results and Discussion

To evaluate how cloud types organize the balance among multiple SIP mechanisms, we define basic cloud types in terms of two controls on the microphysical regime of the mixed-phase region: ascent (convective versus stratiform) and whether the warm rain or ice crystal process of precipitation prevails, for which cloud-base temperature serves as the proxy. The four basic cloud types are thus warm- and cold-based convective and stratiform clouds (Table 1), represented by four observed cases from past field campaigns: stratiform cloud with a slightly cold base (ACAPEX) and convective clouds with cold (STEPS), warm (MC3E) and very warm (GOAmazon) bases (Sec. 4).

Inevitably, several basic cloud types co-exist in each simulation, because the 3D domain is of mesoscale extent and because in nature one cloud type creates others under the same atmospheric forcing (an MCS, for example, involves stratiform and cirriform cloud from the outflow of many deep convective cells). We therefore classify each cloudy grid point by its vertical velocity rather than assigning a whole case to one type; since different cloud types nevertheless predominate in different mesoscale cloud ensembles, comparison among the contrasting cases elucidates how cloud types organize the SIP pathways. The control simulations, the aerosol loadings used to initialize the AC model, and the comparison with coincident aircraft and ground-based observations are described in the Supplementary Information (Secs. 4.3, S2 and S3; Figs. S1–S5).

2.1 Vertical profiles of ice enhancement by each SIP mechanism in the basic cloud types

Figures 2 and 3 show vertical profiles of the IE ratio (the ratio of total ice number concentration, excluding homogeneously nucleated ice, to that of active INPs) and of the ice concentration attributed to each SIP mechanism, for the cloud type that predominates in each case: stratiform for ACAPEX and convective for STEPS, MC3E and GOAmazon. The profiles are averages over all cloudy grid points throughout the cloud life cycle and therefore characterize the mean dependence of ice enhancement on cloud-base temperature and vertical motion in each regime. They reveal marked contrasts among the four regimes in the mechanisms responsible for ice enhancement, reflecting differences in cloud-base temperature, vertical motion, and the availability of supercooled liquid water. The corresponding profiles for the non-predominant cloud type in each case are given in Supplementary Figs. S6 and S7. The following subsections examine each cloud type in turn, followed by a comparison of the SIP mechanisms across the four regimes.

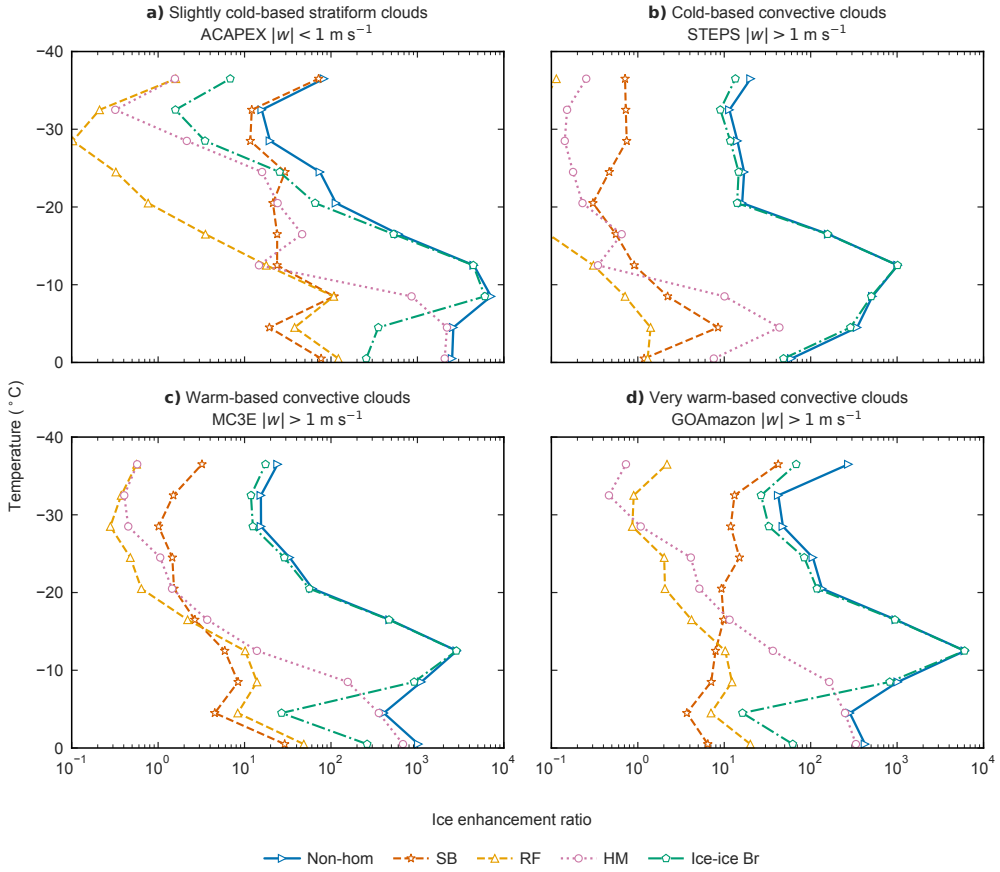


Fig. 2 Vertical profiles of total IE ratio for non-homogeneous ice from all SIP mechanisms (blue right-pointing triangle, "Non hom") are shown, conditionally averaged over stratiform (a) ACAPEX, and convective (b) STEPS, (c) MC3E, and (d) GOAmazon clouds regions for four cases. Also, shown are individual contributions from the four SIP mechanisms, namely sublimational breakup ('SB'; red stars), raindrop-freezing fragmentation ('RF'; yellow upward-pointing triangles), HM process ('HM'; mauve circles), and ice-ice collisional breakup ('Ice-ice BR'; green pentagon). IE ratio is calculated using primary ice estimated from the in-cloud local values of the prognostic variables from the EP scheme for all INPs lost by activation (see [41]).

2.1.1 Slightly Cold-Based Stratiform Clouds

Figure 3a shows concentrations of total ice, primary ice, non-homogeneous ice and the components from each SIP mechanism, averaged over the slightly cold-based stratiform cloud of the ACAPEX simulation; the embedded weak convective cells are treated in Figs. S6a and S7a. The average IE ratio in the stratiform cloud is dominated by breakup in ice–ice collisions, at about 10^3–10^4 in the lower half (0 to −18 °C) of the mixed-phase region, declining with height to less than 10 towards its top (Fig. 2a).

The HM process contributes a peak IE ratio of 10^3 in and below its generation region (Fig. 2a), with similar values extending slightly higher in the embedded weak convection (Fig. S6a). The height of this peak agrees with the aircraft observations of Bower et al.[36] (their Fig. 1g,h) in large-scale mixed-phase maritime stratiform cloud, which show a peak IE ratio near −6 °C attributed to the HM process, although the observed values of at least 10^4 exceed the simulated peak by about an order of magnitude. Despite the recent laboratory doubt about the efficiency of the HM process [18], this agreement in the level of the peak supports its representation in the model. Raindrop-freezing fragmentation contributes an IE ratio of 10–100 below the −18 °C level, and sublimational breakup 10–10^2 (Fig. 2a), because the weak ascent and descent of the stratiform cloud do not sublimate its fragments completely.

2.1.2 Cold-Based Convective Clouds

In the cold-based convective clouds of the STEPS simulation, breakup in ice–ice collisions is the only influential SIP mechanism, producing 0.1–100 L^{-1} of ice (Fig. 3b) and an IE ratio of 10–10^3 at all temperatures (Fig. 2b). The HM process and sublimational breakup yield average IE ratios of less

than 10 and 3, respectively (Figs. 2b and S6b), and the ice concentrations from these two mechanisms and from raindrop-freezing fragmentation are all lower than that of primary ice everywhere above about the −10 °C level (Fig. 3b), so none of them dominates ice production at any level. The reason is that the cold cloud base and continental aerosol conditions prevent coalescence, so there are no supercooled raindrops and hence little 'warm' graupel from raindrop freezing; indeed, no supercooled rain was seen in cloud in the optical-probe imagery from the T-28 aircraft flights [24].

Sublimational breakup and the HM process cause little ice enhancement and have average IE ratios less than 3 and 10, respectively (Figures 2b and S6b) for this basic cloud-type. So, breakup in ice-ice collisions is the leading SIP mechanism with IE ratios of 10^1 to 10^3 in cold-based convective clouds.

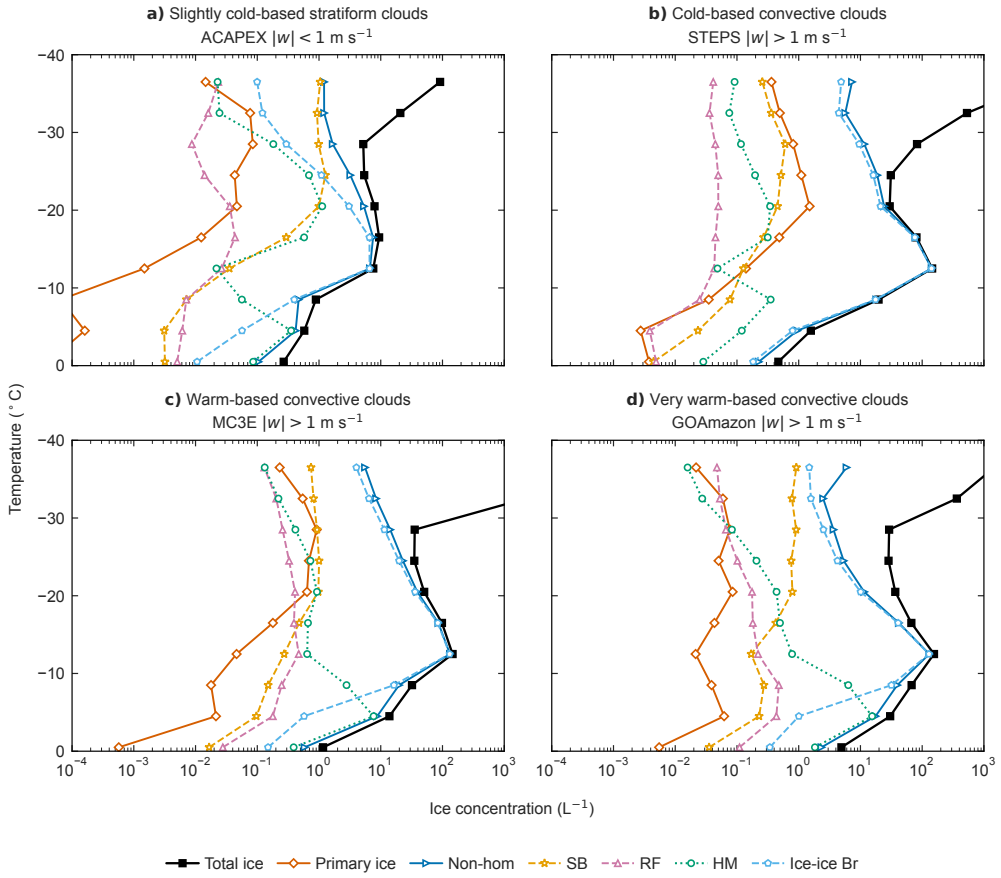


Fig. 3 Vertical profiles of total ice concentrations ('Total ice'; black squares) and their contribution from 'non-homogeneous' ice not initiated by homogeneous freezing ('Non-hom'; blue right-pointing triangles) are displayed, conditionally averaged over all stratiform (a) ACAPEX and convective (b) STEPS, (c) MC3E, and (d) GOAmazon cloudy regions. Also shown are the components from heterogeneously nucleated primary ice ('Primary ice'; crimson diamonds), and the four SIP mechanisms, plotted as in Fig. 2

2.1.3 Warm-Based Convective Clouds

In the warm-based convective clouds of the MC3E simulation, the HM process dominates the secondary ice concentration below the −8 °C level, where cloud droplets large enough to rime-splinter coexist with graupel: its IE ratio peaks at about 10^3 (Fig. 2c), with an ice concentration of about 10 L^{-1} (Fig. 3c). Above the −8 °C level, breakup in ice–ice collisions dominates the total non-homogeneous ice concentration of 3–10 L^{-1} (Fig. 3c).

Raindrop-freezing fragmentation has an IE ratio of less than about 20 in the lower half of the mixed-phase region and is absent from the upper half (Fig. 2c), because the average cloud-droplet diameter rarely exceeded 20 μm (Fig. S4c), curbing coalescence under the continental aerosol conditions of a cloud base that was not especially warm. Sublimational breakup is similarly weak, with a peak IE ratio of about 25, but is more prolific than raindrop-freezing fragmentation (Figs. 2c and 3c).

2.1.4 Very Warm-Based Convective Clouds

In the very warm-based convective clouds of the GOAmazon simulation, all four SIP mechanisms are active throughout the mixed-phase region (0 to −36 °C). Above the −30 °C level the ice concentrations from ice–ice collisional breakup and sublimational breakup are comparable, at about 100 L^{-1}, with collisional breakup producing roughly twice as much (Figs. 3d and S7d).

Sublimational breakup yields average IE ratios of about 10–10^2 (Figs. 2d and S6d), with particularly strong enhancement in convective downdrafts, where fragments accumulate and subsequently mix into the surrounding cloud [17].

As in the other cases, the HM process and raindrop-freezing fragmentation show a similar height dependence, with IE ratios that decline with height and are appreciable mainly in the lower half of the mixed-phase region. The HM process dominates within the rime-splintering temperature range, with an IE ratio of about 10^2, but its ice concentration exceeds that of primary ice only below the −20 °C level (Fig. 3d). Raindrop-freezing fragmentation is sustained by the prolific warm-rain production, but its IE ratio stays below that of the HM process because relatively little warm rain is transported above the freezing level (Fig. 2d).

2.1.5 Comparison Among Cloud-types

Across the four cases, the simulated HM process depends strongly on cloud-base temperature, owing to its requirement for cloud droplets larger than 24 μm in the HM region: in terms of IE ratio it is comparably important in convective and stratiform clouds but more active in warm-based than in cold-based clouds. Raindrop-freezing fragmentation likewise is nearly absent in cold-based clouds and active in warm-based ones (Secs. 2.1.2 and 2.1.4).

By contrast, breakup in ice–ice collisions depends more on cloud dynamics (convective versus stratiform) than on cloud-base temperature. Sublimational breakup produces only modest ice enhancement in the stratiform ACAPEX case and is substantially more active in the warm-based convective cases than in the cold-based one (Fig. 2b,c). Finally, in all four cases homogeneously nucleated ice is transported downward and dominates the total ice concentration throughout much of the upper half of the mixed-phase region.

2.2 Distribution of simulated ice enhancement in dynamical–thermodynamic phase space

To compare the ice multiplication mechanisms among the basic cloud types, we next analyze cloud glaciation in a phase space of vertical velocity and subzero temperature (w–T space), binning every cloudy grid point of the 3D domain by its local dynamical and thermodynamic conditions. Whereas the vertical profiles above (Sec. 2.1) give only the height dependence of domain-wide glaciation, this w–T map shows how the SIP mechanisms are organized by temperature and vertical motion together, how the basic cloud types occupy distinct regions of the phase space, and how updrafts and downdrafts are linked in their microphysical evolution.

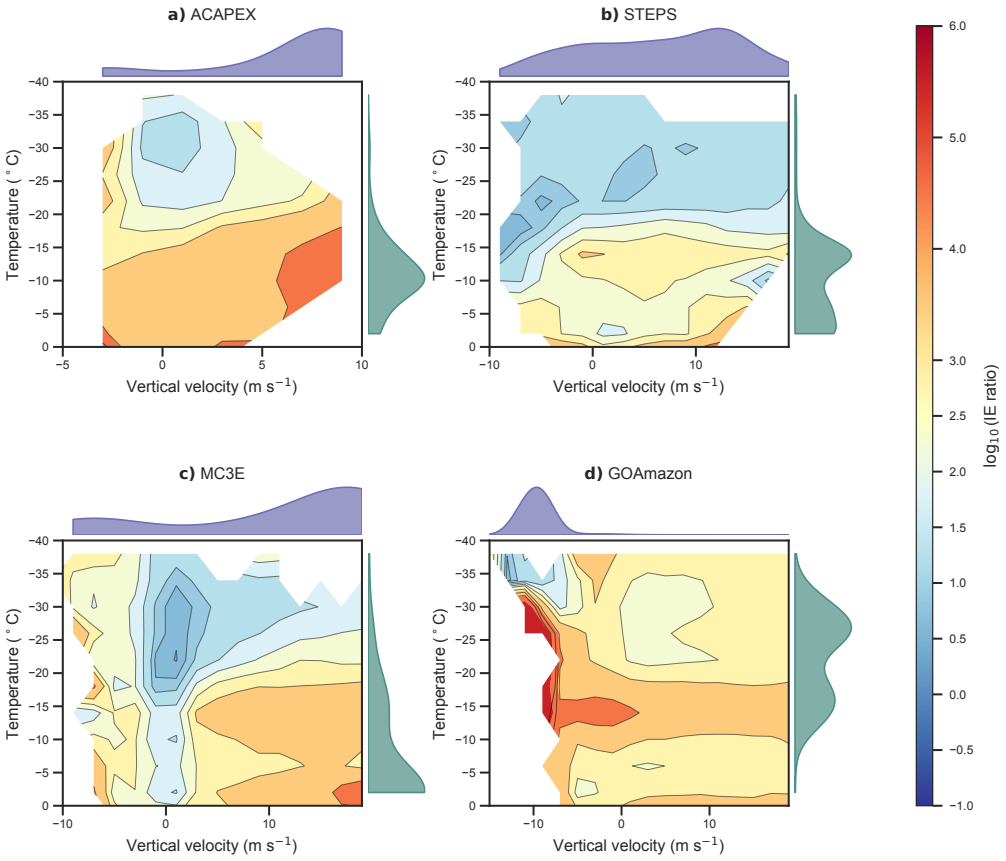


Fig. 4 w–T maps of total IE ratio for (a) the slightly cold-based stratiform clouds of ACAPEX, (b) the cold-based convective clouds of STEPS, (c) the warm-based convective clouds of MC3E and (d) the very warm-based convective clouds of GOAmazon. The marginal distributions above and to the right of each panel show the IE-weighted distribution of grid points across vertical velocity (purple) and across temperature (teal).

Figure 4 shows the w–T maps of total IE ratio for the four cases. In the slightly cold-based stratiform case (ACAPEX), ice enhancement is strongest at relatively warm mixed-phase temperatures and generally increases with ascent, consistent with weaker precipitation production aloft. In the convective cases, enhancement peaks near −15 °C, and GOAmazon shows substantially stronger enhancement over a broader range of w and T, with IE ratios of 10^2–10^3 spanning much of the mixed-phase region. The warm-based convective cases also show strong enhancement (IE ratios $> 10^3$) in their downdrafts (Fig. 4c,d), which the tagged maps below attribute to sublimational breakup, whereas this feature is much weaker in ACAPEX. The following subsections examine the contribution of each SIP mechanism, from the tagging tracers, for each basic cloud type.

2.3 Slightly cold-based stratiform clouds in w–T space

Figure 5 shows the w–T maps of the IE ratio from each SIP mechanism in the slightly cold-based orographic clouds over the Sierra Nevada in ACAPEX. There is no absolute separation between stratiform and convective cloud in nature: as commonly observed [42], cells of very weak convection (about 1–2 m s^{-1}) are embedded in decks of deep mixed-phase nimbostratus and generate precipitation that falls into the stratiform cloud, and these embedded cells shape the maps below.

Breakup in ice–ice collisions is vigorous in the stratiform regions ($|w| < 1$ m s^{-1}) from −5 to −38 °C, with a broad peak in IE ratio of about 10^3 near −15 °C, and it intensifies with ascent from 0 to a few m s^{-1} in the embedded cells, because faster ascent lofts more precipitation and boosts the cloud liquid available for its accretional growth (Fig. 5c).

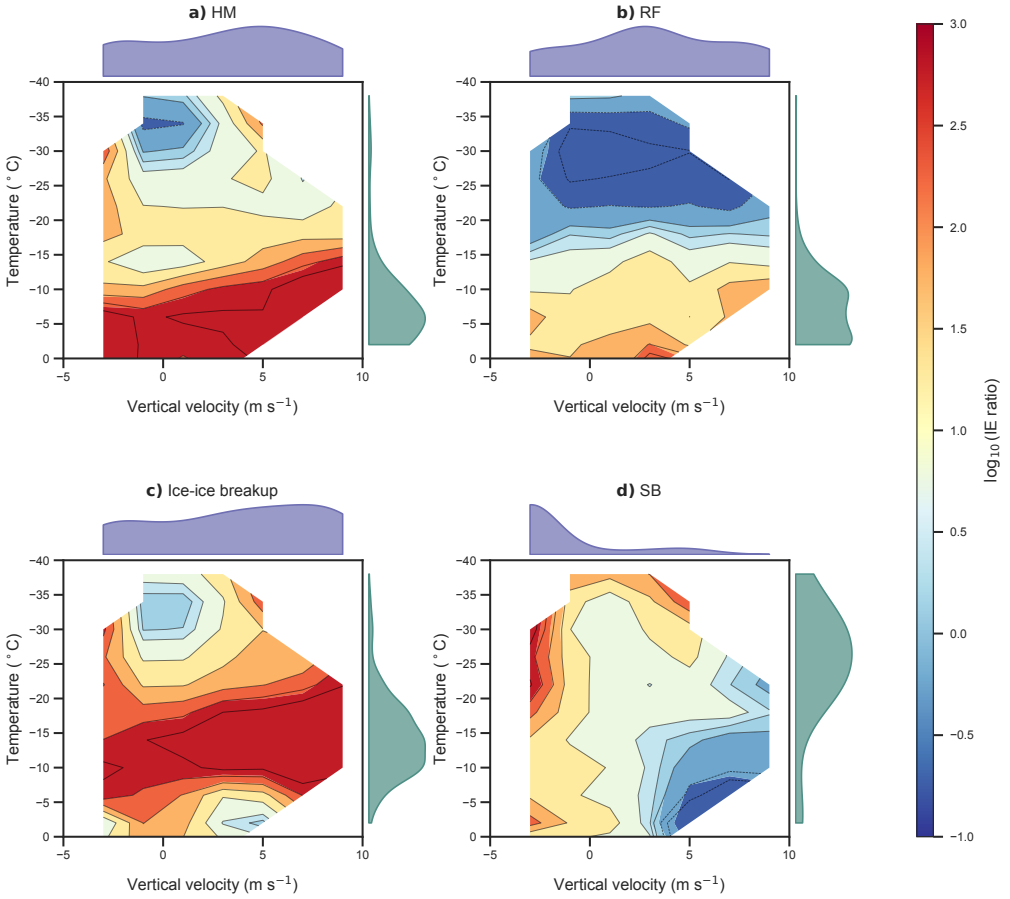


Fig. 5 IE ratio, plotted logarithmically on a w–T map, for the slightly cold-based stratiform clouds of the ACAPEX simulation, from (a) the HM process, (b) raindrop-freezing fragmentation (RF), (c) breakup in ice–ice collisions and (d) sublimational breakup. Values of the logarithm of the IE ratio below zero represent no appreciable ice enhancement.

The HM process contributes intensely from 0 to −10 °C, with a peak IE ratio of up to 10^3 near −6 °C that likewise increases with the weak ascent of the embedded cells (Fig. 5a); as noted above (Sec. 2.1.1), this mirrors the peak observed by Bower et al.[36] (their Fig. 1g,h). In the upper half of the mixed-phase region, however, its IE ratio is mostly below 10, especially near zero ascent. The HM process exceeds raindrop-freezing fragmentation throughout the map, although the two follow a qualitatively similar pattern, and is itself exceeded only by sublimational breakup in the upper half of the mixed-phase region.

Sublimational breakup is active there in the weak convective descent of the embedded cells and the associated stratiform cloud aloft, with an IE ratio exceeding 10 (Fig. 5d). A larger share of its fragments is recirculated into the stratiform and weak embedded ascent than in the convective cases examined below (Secs. 2.4–2.6).

Raindrop-freezing fragmentation is the weakest mechanism in the upper half of the mixed-phase region (Fig. 5b), but below the −15 °C level, in the stratiform ascent and the embedded convection, it ranks third with an IE ratio above 10. This is because the upstream cloud base (8 °C) is not cold enough, under the maritime aerosol conditions, to shut off the warm rain process entirely, so a limited amount of supercooled rain forms aloft.

2.4 Cold-Based Convective Clouds in *w*-*T* Space

Figure 6 shows the w–T maps of the IE ratio from each SIP mechanism in the cold-based convective clouds of the STEPS simulation. In contrast with the other three cases, breakup in ice–ice collisions is the only vigorous source of secondary ice (Fig. 6c). Most of its fragments are concentrated around a peak near −15 °C (IE ratio of about 10^2), as expected for fragile snow in the dendritic regime (−12 to −17 °C), and in the upper half of the mixed-phase region its IE ratio increases with updraft speed as more precipitation is supported aloft. The HM process, raindrop-freezing fragmentation and sublimational breakup (Fig. 6a, b and d) are almost absent over most of the map, with IE ratios

below unity, that is, less ice than the primary ice from active INPs. The two exceptions are modest IE ratios of about 10 in and below the HM generation region (−3 to −8 °C), decreasing with increasing ascent, and much higher IE ratios (10^2–10^3) from sublimational breakup in fast convective descent at similar levels, whose fragments mix slightly into the convective ascent there.

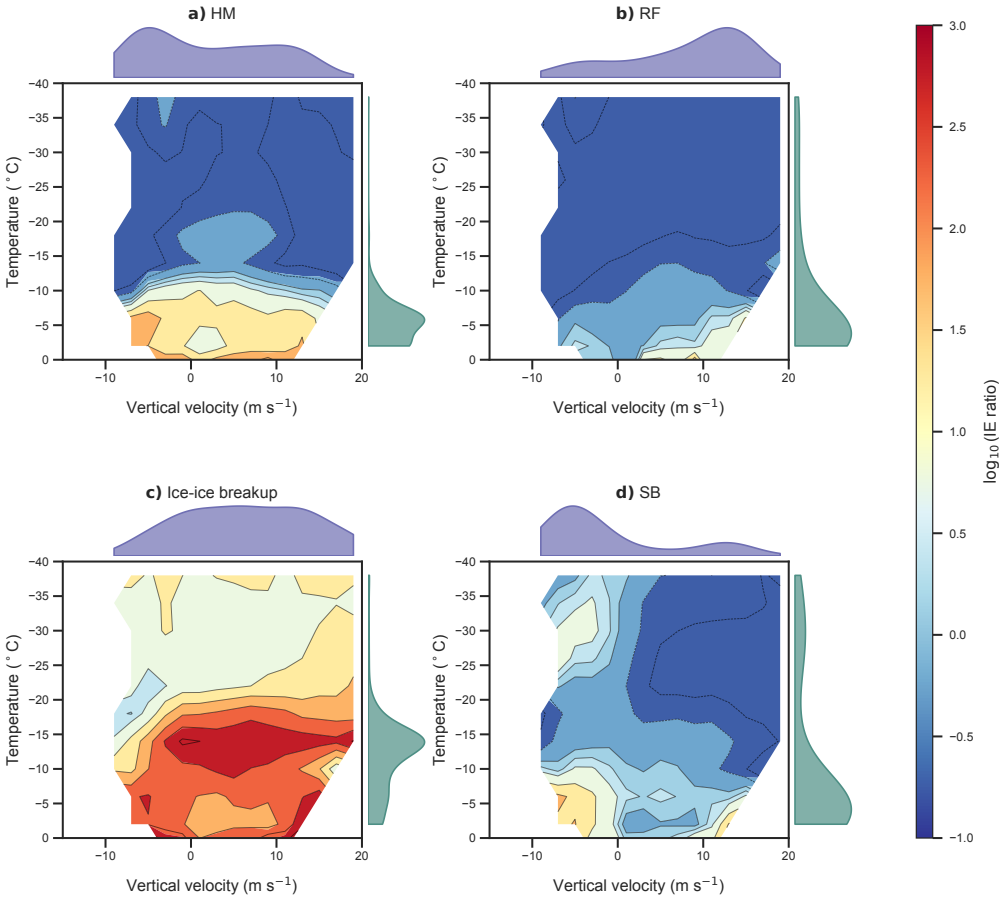


Fig. 6 IE ratio on a w–T map for the cold-based convective clouds of the STEPS simulation, from (a) the HM process, (b) raindrop-freezing fragmentation (RF), (c) breakup in ice–ice collisions and (d) sublimational breakup.

2.5 Warm-based convective clouds in w–T space

Figure 7 shows the w–T maps of the IE ratio from each SIP mechanism in the warm-based convective clouds of the MC3E case (Sec. 4.3.3). Breakup in ice–ice collisions is the most prolific mechanism between −5 and −38 °C over almost all vertical velocities simulated, with its IE ratio peaking near −15 °C as in the other cases (Fig. 7c).

As in the other cases, the HM process and raindrop-freezing fragmentation have qualitatively similar maps, both generally increasing with the speed of ascent or descent (Fig. 7a,b). This is consistent with faster updrafts supporting more cloud liquid and precipitation mass aloft [22, 43] through faster condensation, since both mechanisms require cloud droplets above a size threshold (about 24 μm for the HM process; about 20 μm for coalescence to form rain). Both are also accelerated by the freezing of supercooled raindrops on collision with secondary ice splinters (e.g., Phillips et al.[10], their Fig. 7), which produces graupel instantly and circumvents the lengthy vapor growth of crystals followed by riming [44]. The HM process is more active here than in the cold-based case above, and exceeds raindrop-freezing fragmentation throughout the map. Its IE ratio decreases with increasing "distance" on the map from its source region, the convective ascent between −3 and −8 °C, illustrating a convective "diffusion" of ice concentration through w–T space.

Sublimational breakup shows ice enhancement of up to 10^2 in the fastest convective downdrafts but little in either the stratiform or the convective ascent (Fig. 7d), consistent with weaker diffusion, such as by recirculation from downdrafts into updrafts, than in the other cases.

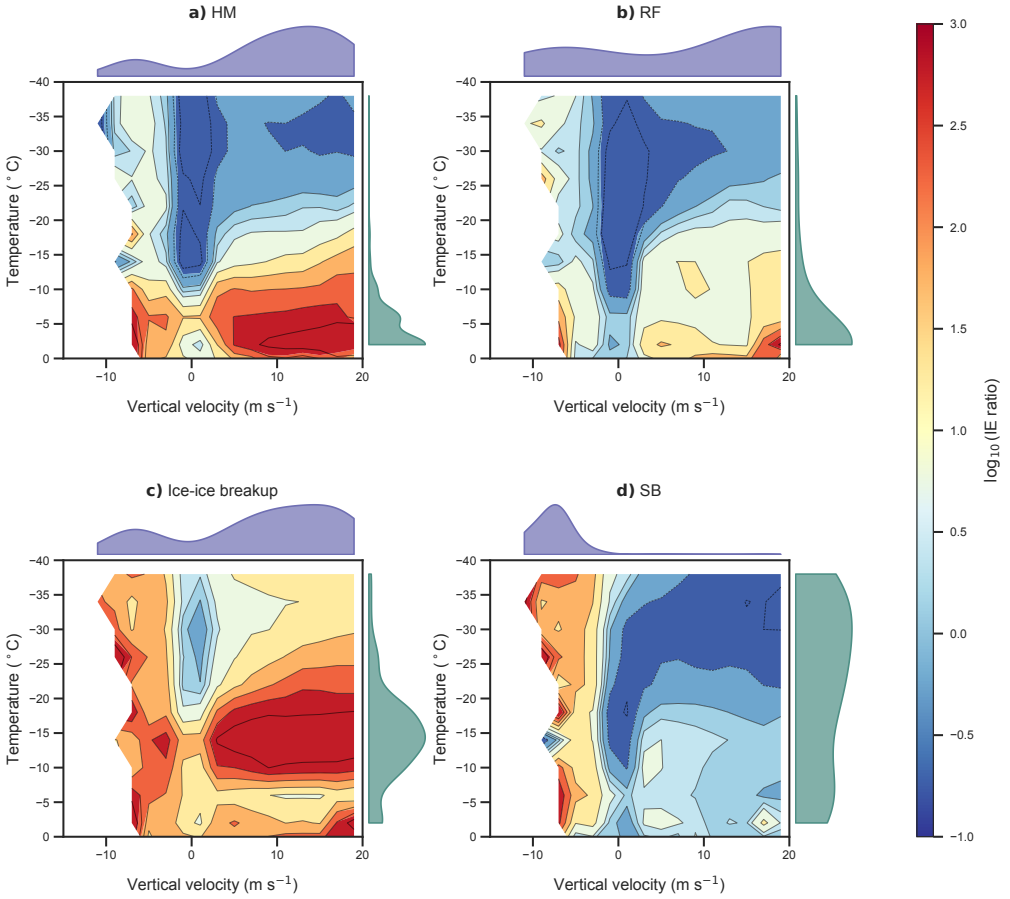


Fig. 7 IE ratio on a w–T map for the warm-based convective clouds of the MC3E simulation, from (a) the HM process, (b) raindrop-freezing fragmentation (RF), (c) breakup in ice–ice collisions and (d) sublimational breakup.

2.6 Very Warm-Based Convective Clouds in *w*-*T* Space

Figure 8 shows the w–T maps of the IE ratio from each SIP mechanism in the very warm-based convective clouds of GOAmazon over Amazonia. Breakup in ice–ice collisions produces even larger ice enhancement than in the convective cases with less warm bases, and its ice concentration is more nearly uniform across the w–T space of the mixed-phase region, not being restricted to any particular range of subzero temperatures (Fig. 8c): fragments are upwelled from the peak of fragile ice in the dendritic region near −15 °C, increasingly so with faster ascent.

The HM process and raindrop-freezing fragmentation show ice enhancement throughout the lower half of the mixed-phase region at all vertical velocities, exceeding that in the warm-based MC3E case (Fig. 8a,b). Both IE ratios increase only weakly with updraft speed, as expected from the lofting of splinters, supercooled rain and large droplets for coalescence, and both have a minimum in the upper half of the mixed-phase region in stratiform cloud near $w = 0$. The vertical extent of enhancement from raindrop-freezing fragmentation is greater in convective than in stratiform ascent, consistent with faster upwelling of supercooled drops. Across the three convective cases, the ice enhancement from the HM process intensifies as the cloud base warms from cold to very warm.

Sublimational breakup produces an IE ratio of up to 10^3 in the convective downdrafts of this tropical case throughout the depth of the mixed-phase region, as expected from the need for descent to create sufficient subsaturation with respect to ice [17] (Fig. 8d). The abundant graupel generated by the warm rain process and raindrop freezing in convective ascent, combined with strong shear aloft, makes this sublimation more intense than in the cold- and warm-based convective cases. In convective ascent of up to 10 m s^{-1} the IE ratio is only marginally above unity, from sublimational fragments diffusing into the faster updrafts.

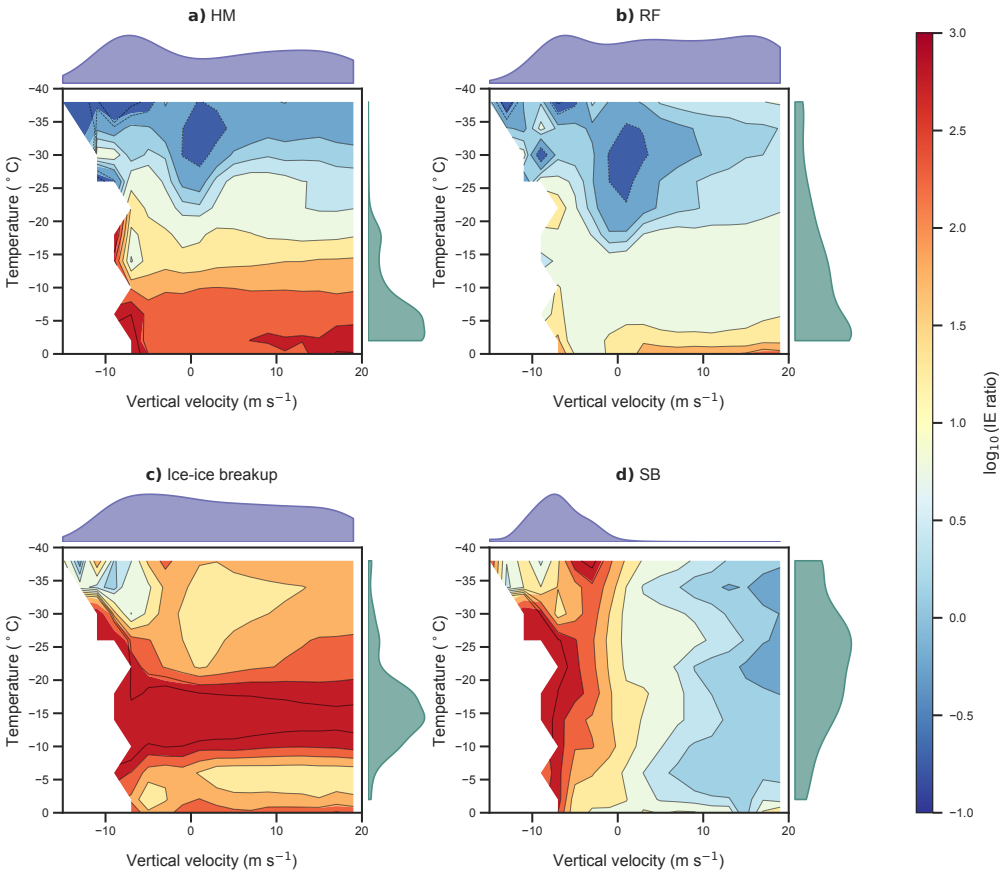


Fig. 8 IE ratio on a w–T map for the very warm-based convective clouds of the GOAmazon simulation, from (a) the HM process, (b) raindrop-freezing fragmentation (RF), (c) breakup in ice–ice collisions and (d) sublimational breakup.

2.7 Cumulative Budget Analysis

Budgets were constructed by counting all ice particles produced by each pathway over the entire simulation and 3D domain. Figure 9 shows the relative numbers of non-homogeneous ice particles so produced in the four cases, and the ranking of the SIP mechanisms is the same in all four basic cloud types. The fractional contribution from breakup in ice–ice collisions is largest in the cold-based convective clouds of STEPS, at about 96% of all ice produced in the storm, followed by the warm-based convective clouds of MC3E and then the very warm-based convective clouds of GOAmazon (Fig. 9b–d). This trend arises because, although the absolute number of particles from collisional breakup decreases only mildly as the cloud base cools from GOAmazon to STEPS, the other three mechanisms decrease much more and are almost shut down, since all three require large cloud droplets in the lower half of the mixed-phase region, partly through the warm rain process (Fig. S8) and the associated formation of 'warm' graupel by raindrop freezing. The slightly cold-based stratiform clouds of ACAPEX conform to the same trend (Fig. S8).

Sublimational breakup makes a prolific contribution to the budget of the convective cloud types, and its contribution increases with cloud-base temperature among the four cases (STEPS < ACAPEX < MC3E < GOAmazon). Although most of its fragments sublimate away completely, the fraction that survives is predicted to increase with the warmth of the cloud base among the convective cases.

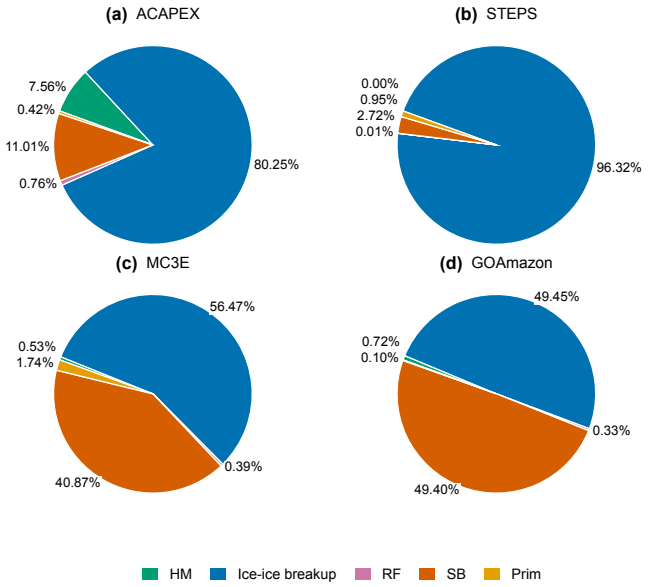


Fig. 9 Total numbers of ice particles produced, throughout each control simulation and over the entire 3D domain, by each non-homogeneous source for (a) ACAPEX, (b) STEPS, (c) MC3E and (d) GOAmazon. The sources are primary ice (grey) and the SIP mechanisms of the HM process (green), breakup in ice–ice collisions (blue), raindrop-freezing fragmentation (purple) and sublimational breakup (vermillion). For sublimational breakup, only the fragments that survive complete sublimation are shown; this fraction is obtained from the tagging tracer for sublimational-breakup ice, which also budgets the fragments lost by complete sublimation, so that the number surviving is the total produced minus the number lost.

3 Discussion

The four basic cloud types were simulated with the AC model for cases observed in the ACAPEX, STEPS, MC3E and GOAmazon campaigns, using the aerosol conditions observed in each (Tables 1 and 2; Sec. 1), and validated against coincident aircraft and ground-based observations across a range of microphysical and dynamical properties (Figs. S2–S5; Sec. S3). Tagging tracers attribute every ice particle to the SIP mechanism that produced it, and the mechanisms are ranked by the simulation-averaged concentration of ice attributed to each. On that measure the hierarchy is the same in all four cloud types: breakup in ice–ice collisions is the leading contributor to ice production, followed by sublimational breakup, the HM process, and raindrop-freezing fragmentation. The central result is that this activity is organized chiefly by cloud-base temperature, which controls which mechanisms are available, and by vertical velocity, which controls where in the cloud they operate.

Ice–ice collisional breakup dominates wherever sufficient ice precipitation is present, over a broad range of temperatures and vertical velocities, and its importance increases strongly with ascent. In the simulated deep convection its ice enhancement peaks near −15 to −25 °C, reaching local IE ratios of 10^3–10^4 in strong updrafts. The mechanism is sustained by graupel and hail grown through riming and raindrop freezing, which supply large particles for energetic collisions with snow, and it is not restricted to particular temperatures or humidities: mixed-phase conditions are needed somewhere in the cloud to produce the graupel and hail, but not locally where the breakup occurs. This makes it the most robust SIP mechanism across the simulated cloud types.

Cloud-base temperature controls the availability of the other pathways by regulating warm-rain production, droplet growth, and the formation of supercooled rain and graupel, so that warmer-based clouds support greater activity of all SIP mechanisms. In the continental convective cases with cold or moderately warm bases (STEPS, MC3E) the ice-crystal process of precipitation dominates, whereas in the very warm-based tropical case (GOAmazon) the warm-rain process prevails [21], and the warmer-based clouds show the greater ice enhancement from ice–ice breakup, consistent with an extra contribution from ‘warm’ graupel formed by raindrop freezing aloft. The HM process, which requires cloud droplets larger than about 24 μm and graupel in the −3 to −8 °C generation region, intensifies with cloud-base warming among the cases: it is negligible in the cold-based STEPS case, where droplets remain too small, and strongest in the lower mixed-phase region under aerosol conditions that favor large droplets, such as the maritime environment of ACAPEX. Raindrop-freezing fragmentation likewise becomes possible in warmer-based clouds and follows the spatial distribution

of the HM process, but its ice enhancement is one to two orders of magnitude smaller, with IE ratios of up to about 10. In cold-based convection the warm-rain pathway is suppressed, leaving collisions of snow with 'cold' graupel, grown by riming of snow, as the principal source of ice enhancement.

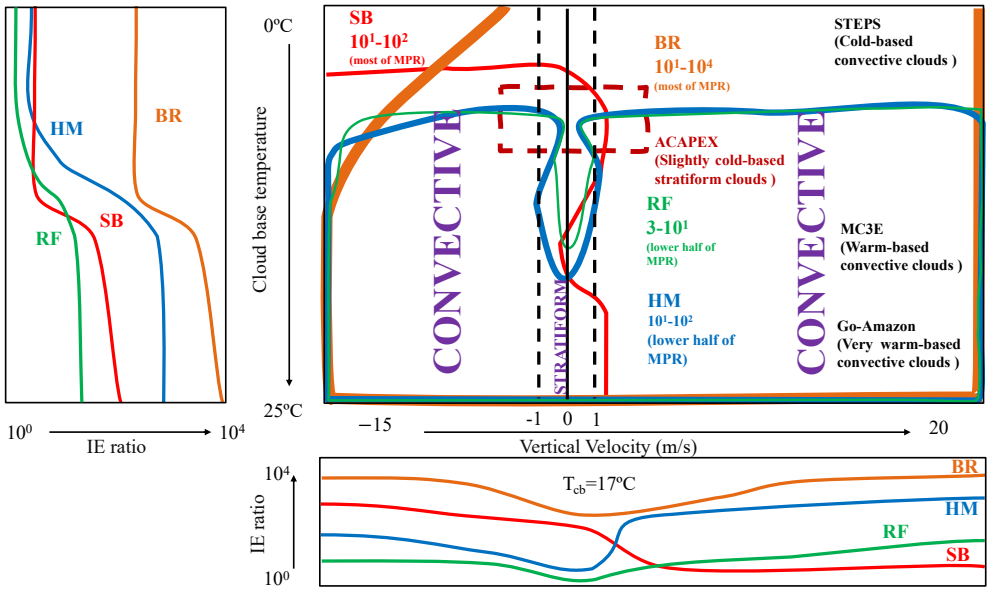


Fig. 10 Schematic diagram of how SIP mechanisms are organized by cloud-base temperature and vertical velocity, reflecting results from the AC simulations in the present paper. The central map shows the realm of activity of each SIP mechanism enclosed by a coloured contour, with contour thickness denoting qualitatively the relative strength of the mechanism: the HM process of rime splintering ('HM', blue), breakup in ice–ice collisions ('BR', yellow), raindrop-freezing fragmentation ('RF', green) and sublimational breakup ('SB', red), each shown with its expected range of IE ratio. 'MPR' denotes the mixed-phase region. The lower panel sketches how the IE ratio depends on vertical velocity for a typical cloud-base temperature (T_{cb}) of 17 °C, and the right panel how it depends qualitatively on cloud-base temperature, generalizing over all vertical velocities. Where a contour overlaps an axis of the schematic, that boundary is open.

Vertical velocity determines where the mechanisms operate. Strong ascent promotes supercooled cloud liquid, riming and graupel/hail growth, and suspends larger graupel and hail aloft for energetic collisions with snow, so ice–ice breakup strengthens in faster updrafts; the HM process is also favored by ascent through enhanced droplet growth and is most influential in the lower mixed-phase region. Sublimational breakup occupies a distinct dynamical regime, requiring downdrafts of at least 2–3 m s^{-1}, where local IE ratios reach 10^3 in MC3E and ACAPEX and 10^6 in GOAmazon. Only a small fraction of the fragments generated in these subsaturated downdrafts escape complete sublimation, as our tracer budget of the fragments that sublimate away shows, but the production rate, mostly from sublimating graupel, is large enough that the survivors remain significant in absolute terms. Once carried into adjacent saturated air, by turbulent or convective mixing or when dilute downdrafts reach their level of neutral buoyancy within the cloud, these fragments grow and are mixed through the rest of the cloud, so that sublimational breakup influences regions well beyond the downdrafts that generate it, as envisaged by Deshmukh et al.[17]. Consequently it competes with ice–ice breakup in the upper mixed-phase region of the warmest-based cases despite its low local survival fraction, dominates the ice enhancement at −25 to −40 °C in the slightly cold-based stratiform case (ACAPEX), and is almost as influential as ice–ice breakup in the warmer-based cases, where fragments survive convective descent, mix into adjacent ascent, and graupel aloft is prolific.

Figure 10 summarizes this organization in cloud-base-temperature/vertical-velocity space: warmer cloud bases favor SIP by enhancing warm-rain production, supercooled cloud liquid, supercooled rain aloft and graupel formation, which boost all the simulated mechanisms of fragmentation. The stronger ascent also boost supercooled cloud liquid and supports growth of precipitation which favors collisional breakup and the HM process, while strong descent promotes sublimational breakup. Raindrop-freezing fragmentation extends over a deeper layer as cloud-base temperature increases but remains a modest source throughout the phase space. Regarding the role of ascent, Fig. 10 highlights how stratiform cloud types with weak ascent have weak HM process and raindrop freezing fragmentation compare to convective cloud types while sublimational breakup is restricted to the downdraft of convective cloud types, whereas ice–ice collisional breakup is ubiquitous in all the cloud types.

The findings carry two implications. First, Models that represent SIP by the HM process alone [4] omit the two leading mechanisms in every cloud type simulated here. The recent experiment doubts about whether the HM process being significant [18] bears mainly on the lower mixed-phase region of warm-based clouds rather than on total ice production. Secondly, since sublimational breakup acts on the wider cloud through fragments exported from downdrafts, its signature should be sought at the margins of convective and stratiform downdrafts rather than within them in the future studies.

These conclusions are subject to the SIP parameterizations used here. Laboratory characterization is limited for sublimational breakup and raindrop-freezing fragmentation, and now contested for the HM process [18], and the bulk microphysical treatment cannot represent the full range of particle properties and spatial scales in real clouds. Nevertheless, the consistent organization of SIP across four contrasting cloud types indicates that cloud-base temperature and vertical velocity provide useful first-order controls on the relative activity of the multiplication pathways. This Part I has established that baseline organization; Part II builds on it by examining the sensitivity of ice multiplication to environmental factors and the interactions among the microphysical pathways.

4 Methods

4.1 Basic cloud types

Corresponding to the target 'basic cloud-types' (Table 1), field campaigns were selected to simulate these cloud-types as far as possible. Table 2 lists these with their cloud base temperature, maximum ascent and aerosol conditions. The cloud base temperature determines which of both precipitation processes ('warm' and 'cold') prevails, with some influence also from aerosol conditions (Section 1). Generally, the warm rain process tends to prevail in clouds with a very warm base [21] while the ice crystal process of precipitation typically prevails in cold-based clouds [24]. It was not possible to find any observed case here to represent a warm-based stratiform cloud type.

Simulated case	T_{cb} (°C)	w_{max} (m/s)	Aerosol conditions	Dominant cloud type
ACAPEX	7	2	Maritime	Slightly cold-based stratiform
STEPS	0	14	Continental	Cold-based convective
MC3E	17	11	Continental	Warm-based convective
GOAmazon	25	20	Continental	Very warm-based convective

Table 2 Dominant cloud types and their classification with cloud base temperature (T_{cb}), maximum vertical velocities (w_{max}, cumulative frequency of 1%), and aerosol input conditions for simulations in the four cases simulated here.

4.2 Framework of the Aerosol–Cloud (AC) Model

The Aerosol–Cloud (AC) model was developed by Phillips et al.[45] within the Weather Research and Forecasting (WRF) framework as a cloud-resolving model with prognostic treatment of several aerosol species. AC couples cloud microphysics with aerosol chemistry through a hybrid two-moment bulk/bin microphysics scheme, with five hydrometeor species: cloud liquid, cloud ice (crystals), snow, graupel/hail and rain. Emulated bin microphysics is used for coagulation processes [24, 41, 45–49], and the preferential evaporation of the smaller cloud droplets in ascent near −36 °C during homogeneous freezing is treated [41].

Four processes of fragmentation are considered in AC to initiate secondary ice: breakup in ice–ice collisions [24, 48], rime splintering by [8], raindrop freezing fragmentation (modes 1 and 2) [10], and sublimational breakup [17]. More details are given in Supplement section S1.

4.3 Observational field campaigns and model setup

The four field campaigns selected (Sec. 4.1) to exemplify the basic cloud types, namely warm- and cold-based convective or stratiform cloud (Table 1 and 2), are described as follows.

4.3.1 ACAPEX: Slightly cold-based stratiform cloud

The US Department of Energy (DoE) directed an Atmospheric Radiation Measurement (ARM) Cloud Aerosol Precipitation Experiment (ACAPEX) field campaign. The DOE G-1 aircraft sampled clouds over the Sierra Nevada mountain range during the postfrontal scenario on 7 February 2015. The scattered low-level, orographic and mostly stratiform clouds were observed with a dense cloud base at about 1.2 km above mean sea level (MSL), (about 8 °C), upstream from the mountains [50, 51]. The mountains extend up to a ground elevation of about 2.1 km MSL (about -2 °C). The south-westerly flow from the Pacific Ocean passed over the central valley and up over the mountain range, producing a widespread stratiform cloud layer with an upstream cloud base over the valley and extending in contact with the elevated ground over the mountains.

This orographic stratiform cloud case was simulated from the ACAPEX campaign in the Sierra Nevada near Sacramento airport. This case was simulated for a 360 x 80 km domain for 3 hours, considering the topography of the Sierra Nevada mountains with a grid spacing of 2 km horizontally and about 0.5 km vertically. The simulation starts on 7 February 2015 at 19:15 UTC and ends on 22:15 UTC. The domain of ACAPEX is rotated by 31 degrees anticlockwise to make it parallel to the wind direction of the western inflow boundary. Most of the simulation domain includes the mountain

range where the stratiform cloud exists. The lateral boundary conditions are periodic at the northern and southern boundaries and open on the east and west sides of the boundaries.

The validation for CCN and INP activity spectrum for are given in the fig. S1 of supplementary section S3. In figure S2, the microphysical quantities of ACAPEX stratiform cloud are validated.

4.3.2 STEPS: Cold-based convective cloud

A cold-based multicellular convective storm was observed during the Severe Thunderstorm Electrification and Precipitation Study (STEPS) near the Kansas-Colorado border on 19th June 2000 [52]. The cloud base of this multicellular system was located near 0 °C and consisted of different types of clouds like cirriform, stratiform and cumuliform. Flights revealed a general lack of supercooled raindrops aloft, indicative of precipitation from the ice-crystal process. STEPS featured cloud microphysics measurements by the South Dakota School of Mines and Technology's armoured T-28 aircraft. [24] described the microphysical properties of this particular convective system simulated by AC model and evaluated them against the co-incident *in-situ* aircraft, satellite and ground-based observations. The lower troposphere was very dry, causing a lower convective available potential energy (CAPE). Yet, perhaps owing to the high cloud-base and vertical shear, the convection was vigorous enough for hail and graupel aloft.

For the STEPS case, the same multicellular convective system on the evening of 19 June 2000 was simulated using the model setup described by [24]. Simulation starts on 2345 and ends at 0215 UTC. To summarize, the horizontal grid spacing of AC is 1 km and the vertical grid spacing is approximately 0.5 km, with a time step of 10 seconds. The eastern and western sides have open boundary conditions, while the northern and southern sides are periodic. The convective line moves down shear towards the east-north-east (71°C clockwise from north). Therefore, the domain and coordinate system (x and y) of AC were rotated to align the x-axis with this direction, making the convective line parallel to the y-axis. The validation of microphysical properties for the cold-based convective clouds of STEPS are provided in the Supplementary section S3 and Figure S3.

4.3.3 MC3E: Warm-based convective cloud

Warm-based mesoscale convective systems (MCSs) were observed in the Mid-latitude Continental Convective Clouds Experiment (MC3E) on 11th May 2011 over Oklahoma [53]. The cloud base of these MCSs was approximately 17°C and 1.2 km above the ground. The radiosonde observations conducted around 0300 UTC on 10th May had a CAPE of about 3500 J kg^{-1}. The vertical wind shear involved only about 6 m/s of increase from 3 to 13 km altitude above the ground, which is not strong, while the shear in the lowest 3 km involved a change of about 13 m/s. This multicellular convective line was made up of different cloud types, but most of them were cumuliform (e.g., cumulonimbus) and stratiform clouds.

The MC3E case was simulated for 80 x 80 km domain with the grid spacing of 2 km horizontally and about 0.5 km vertically using a time step of 10 seconds. The simulation started at 0000 UTC on 10th May and ended at 0000 UTC on 13th May 2011. Periodic boundary conditions were applied on both eastern-western and northern-southern boundaries. The additional details of experimental setup of this simulation of an MCS and AC model has been evaluated for MC3E case (Figure S4) and more details are given by [26].

4.3.4 GOAmazon: Very Warm-based convective cloud

The Green Ocean Amazon (GOAmazon) campaign was mainly oriented towards the study of the cloud-aerosol interactions in the Amazon Basin. The ARM Mobile Facility was located leeward of the city of Manaus from January 2014 to November 2015 [54]. On 19th March 2014, a MCS was observed from 05 to 19 UTC. In the Amazon region, MCSs frequently occur in the month of March [55–57]. The clouds sampled during GOAmazon had very warm bases (25°C) at about 990 hPa. The radiosonde measured a very high amount of CAPE of about 5000 J kg^{-1} [21]. AC (Section 4.2) was used to simulate this tropical multicellular convective system using a similar model setup as described by [21]. The vertical wind shear of the mean flow was south-westerly, increasing by 22 m/s from 3 to 13 km altitude MSL due to an easterly jet in the lower troposphere and a westerly return flow aloft.

For very warm-based convective clouds of GOAmazon, the grid spacing of AC is 2 km horizontally and about 0.5 km vertically. A time step of 10 s was used in the simulations for a 320 x 80 km domain. To initialize convection in the model, a line consisting of cold, dry bubbles, each with a 10 km horizontal diameter, was used. These bubbles were spaced10 km apart and aligned parallel to the north-south direction (y-axis). The simulation of a convective storm starts at 0500 UTC and completes

around 1900 UTC on 19^{th} March 2014. The eastern-western boundaries are open and northern-southern boundaries are periodic for this simulation. The model was initialized by a radiosonde profile from the GOAmazon campaign observations and validated against the *in-situ* observations (Figure S5).

5 Acknowledgements

This research was supported chiefly by the U.S. Department of Energy's Atmospheric System Research, an Office of Science Biological and Environmental Research program, under DE-SC0018932 award to V. T. J. Phillips (VTJP). This work was guided by VTJP and focused on the modelling of secondary ice initiation in different cloud types. Akash Deshmukh received support also from 'Endowments for the Natural Sciences, Medicine and Technology – Geoscience' from the Royal Physiographic Society of Lund. The work by some other co-authors was also supported by awards to VTJP from the Swedish Research Council (Vetenskapsradet) related to the research of bioaerosol effects on clouds (Award 2015-05104), U.S. Department of Energy (DE- SC0018967), and FORMAS (Award 2018-01795). P. J. DeMott was partially supported by the U.S. Department of Energy's Atmospheric System Research, an Office of Science Biological and Environmental Research program, under DE-SC0021116. Work of Jiwen Fan was supported by the U.S. Department of Energy's Atmospheric System Research. Argonne National Laboratory is operated for the DOE by UChicago Argonne, LLC, under contract DE-AC02-06CH11357. The INP measurements at ATTO Tower were supported by the 7th European Union Framework Programme, BACCHUS, grant No. 603445. We thank Arti Jadav for providing the dataset used in one of the simulations and Sachin Patade for his developement of the model.

- **Conflict of interest/Competing interests**
  The authors declare no competing interests.
- **Data availability**
  The STEPS sounding datasets are freely available from https://data.eol.ucar.edu/project/STEPS. The all data from ACAPEX is available on the given data portal - https://adc.arm.gov/discovery/results/iopShortName::aaf2015acapexaaf. The MC3E ground-based (and aircraft-based) dataset are also freely available and can be obtained using https://ghrc.nsstc.nasa.gov/hydro/details/gpmcmmc3e. The field observational datasets for the GOAmazon can be obtained from https://www.arm.gov/research/campaigns/amf2014goamazon.
- **Code availability**
  All the figures (including Supplementary Figures) are originally produced and plotted using various open-source python libraries.
- **Author Contributions Statement**
  A.D. contributed to conceptualization, methodology, numerical simulations, formal analysis, investigation, writing the original draft, and reviewing and editing the manuscript.V.P. contributed to conceptualization, methodology, investigation, manuscript review and editing, supervision, and funding acquisition. All authors reviewed and approved the final manuscript. D.W. contributed to numerical simulations and manuscript review. A.K.G. contributed to numerical simulations and manuscript review and editing. M.G. contributed to observations of secondary ice production. A.B. contributed to campaign observations and investigation. P.C. contributed experimental data, reviewed and edited the manuscript. G.M. contributed observational data, their interpretation, and manuscript review and editing. P.D. contributed observational campaign data, their interpretation, and manuscript review and editing. J.F. contributed observational data, their interpretation, and manuscript review and editing. Y.L. contributed to observational data. J.S. and H.B. contributed observational datasets and manuscript review and editing.

References

[1] Hobbs, P. V. Ice multiplication in clouds. *Journal of the Atmospheric Sciences* **26**, 315–318 (1969).

[2] Pruppacher, H. R. & Klett, J. D. Microphysics of clouds and precipitation (1997).

[3] Harris-Hobbs, R. L. & Cooper, W. A. Field evidence supporting quantitative predictions of secondary ice production rates. *Journal of the Atmospheric Sciences* **44**, 1071–1082 (1987).

[4] Field, P. *et al.* Chapter 7. secondary ice production–current state of the science and recommendations for the future, meteorol. monogr., american meteorological society, washington, dc, 7.1–7.20 (2017).

[5] Crawford, I. *et al.* Ice formation and development in aged, wintertime cumulus over the uk: Observations and modelling. *Atmospheric Chemistry and Physics* **12**, 4963–4985 (2012).

[6] Taylor, J. W. *et al.* Observations of cloud microphysics and ice formation during cope. *Atmospheric Chemistry and Physics* **16**, 799–826 (2016).

[7] Lawson, R. P., Woods, S. & Morrison, H. The microphysics of ice and precipitation development in tropical cumulus clouds. *Journal of the Atmospheric Sciences* **72**, 2429–2445 (2015).

[8] Hallett, J. & Mossop, S. C. Production of secondary ice particles during the riming process. *Nature* **249**, 26–28 (1974).

[9] Takahashi, C. & Yamashita, A. Production of ice splinters by the freezing of water drops in free fall. *Journal of the Meteorological Society of Japan* **55**, 139–141 (1977).

[10] Phillips, V. T. J., Patade, S., Gutierrez, J. & Bansemer, A. Secondary ice production by fragmentation of freezing drops: Formulation and theory. *Journal of the Atmospheric Sciences* **75**, 3031–3070 (2018).

[11] Vardiman, L. The generation of secondary ice particles in clouds by crystal–crystal collision. *Journal of the Atmospheric Sciences* **35**, 2168–2180 (1978).

[12] Fridlind, A. M. *et al.* Ice properties of single-layer stratocumulus during the mixed-phase arctic cloud experiment: 2. model results. *Journal of Geophysical Research: Atmospheres* **112** (2007).

[13] Yano, J. I. & Phillips, V. T. J. Ice-ice collisions: An ice multiplication process in atmospheric clouds. *Journal of the Atmospheric Sciences* **68**, 322–333 (2011).

[14] Schaefer, V. J. & Cheng, R. J. The production of ice crystal fragments by sublimation and electrification. *Journal de Recherches Atmosphériques* **5**, 5–10 (1971).

[15] Oraltay, R. G. & Hallett, J. Evaporation and melting of ice crystals: A laboratory study. *Atmospheric Research* **24**, 169–189 (1989).

[16] Bacon, N. J., Swanson, B. D., Baker, M. B. & Davis, E. J. Breakup of levitated frost particles. *Journal of Geophysical Research: Atmospheres* **103**, 13763–13775 (1998).

[17] Deshmukh, A., Phillips, V. T. J., Bansemer, A., Patade, S. & Waman, D. New empirical formulation for the sublimational breakup of graupel and dendritic snow. *Journal of the Atmospheric Sciences* **79**, 317–336 (2022).

[18] Seidel, J. S. *et al.* Secondary ice production – no evidence of efficient rime-splintering mechanism. *Atmospheric Chemistry and Physics* **24**, 5247–5263 (2024).

[19] Rogers, R. R. & Yau, M. K. *A Short Course in Cloud Physics* 2 edn (Elsevier, 1989).

[20] Field, P. R. *et al.* Some ice nucleation characteristics of asian and saharan desert dust. *Atmospheric Chemistry and Physics* **6**, 2991–3006 (2006).

[21] Gupta, A. K. *et al.* The microphysics of the warm-rain and ice crystal processes of precipitation in simulated continental convective storms. *Communications Earth & Environment* **4**, 226 (2023).

[22] Phillips, V. T. A theory for the balance between warm rain and ice crystal processes of precipitation in mixed-phase clouds. *Journal of the Atmospheric Sciences* **81**, 317–339 (2024).

[23] Khairoutdinov, M. & Kogan, Y. A new cloud physics parameterization in a large-eddy simulation model of marine stratocumulus. *Monthly Weather Review* **128**, 229–243 (2000).

[24] Phillips, V. T. J. *et al.* Ice multiplication by breakup in ice–ice collisions. part ii: Numerical simulations. *Journal of the Atmospheric Sciences* **74**, 2789–2811 (2017).

[25] Huang, Y. *et al.* Microphysical processes producing high ice water contents (hiwcs) in tropical convective clouds during the haic-hiwc field campaign: evaluation of simulations using bulk microphysical schemes. *Atmospheric Chemistry and Physics* **21**, 6919–6944 (2021).

[26] Waman, D. *et al.* Dependencies of four mechanisms of secondary ice production on cloud-top temperature in a continental convective storm. *Journal of the Atmospheric Sciences* **79**, 3375–3404 (2022).

[27] Waman, D. *et al.* Effects from time dependence of ice nucleus activity for contrasting cloud types. *Journal of the Atmospheric Sciences* **80**, 2013–2039 (2023).

[28] Takahashi, T. & Nagao, Y. Possible high ice particle production during graupel-graupel collisions. *Journal of the atmospheric sciences* **52** (1995).

[29] Phillips, V. T. J. & Patade, S. Multiple environmental influences on the lightning of cold-based continental convection. part ii: Sensitivity tests for its charge structure and land–ocean contrast. *Journal of the Atmospheric Sciences* **79**, 263–300 (2022).

[30] Houze, R. A. *Cloud dynamics* Vol. 104 (Academic press, 2014).

[31] Hallett, J., Sax, R. I., Lamb, D. & Murty, A. S. R. Aircraft measurements of ice in florida cumuli. *Quarterly Journal of the Royal Meteorological Society* **104**, 631–651 (1978).

[32] James, R. L., Phillips, V. T. J. & Connolly, P. J. Secondary ice production during the break-up of freezing water drops on impact with ice particles. *Atmospheric Chemistry and Physics* **21**, 18519–18530 (2021).

[33] Grzegorczyk, P. *et al.* Fragmentation of ice particles: laboratory experiments on graupel–graupel and graupel–snowflake collisions. *Atmospheric Chemistry and Physics* **23**, 13505–13521 (2023).

[34] Gautam, M. *et al.* Fragmentation in collisions of snow with graupel/hail: New formulation from field observations. *Journal of the Atmospheric Sciences* **81**, 2149–2164 (2024).

[35] Blyth, A. M. & Latham, J. Development of ice and precipitation in new mexican summertime cumulus clouds. *Quarterly Journal of the Royal Meteorological Society* **119**, 91–120 (1993).

[36] Bower, K. N. *et al.* A parameterization of the ice water content observed in frontal and convective clouds. *Quarterly Journal of the Royal Meteorological Society* **122**, 1815–1844 (1996).

[37] Sullivan, S. C., Hoose, C., Kiselev, A., Leisner, T. & Nenes, A. Initiation of secondary ice production in clouds. *Atmospheric Chemistry and Physics* **18**, 1593–1610 (2018).

[38] Schumacher, C. & Houze, R. A. Stratiform rain in the tropics as seen by the trmm precipitation radar. *Journal of Climate* **16**, 1739–1756 (2003).

[39] Ritman, M., Jones, W. & Stier, P. Convective controls on anvil cloud evolution in the icon km-scale global climate model. *Atmospheric Chemistry and Physics* **26**, 7105–7126 (2026).

[40] Xu, K. M. Partitioning mass, heat, and moisture budgets of explicitly simulated cumulus ensembles into convective and stratiform components. *Journal of the Atmospheric Sciences* **52**, 551–573

(1995).

[41] Phillips, V. T. J., Donner, L. J. & Garner, S. T. Nucleation processes in deep convection simulated by a cloud-system-resolving model with double-moment bulk microphysics. *Journal of the Atmospheric Sciences* **64**, 738–761 (2007).

[42] Hogan, R. J., Field, P. R., Illingworth, A. J., Cotton, R. J. & Choularton, T. W. Properties of embedded convection in warm-frontal mixed-phase cloud from aircraft and polarimetric radar. *Quarterly Journal of the Royal Meteorological Society* **128**, 451–476 (2002). URL https://rmets.onlinelibrary.wiley.com/doi/abs/10.1256/003590002321042054.

[43] Phillips, V. T. J. Theory of in-cloud activation of aerosols and microphysical quasi-equilibrium in a deep updraft. *Journal of the Atmospheric Sciences* **79**, 1865–1886 (2022).

[44] Chisnell, R. F. & Latham, J. Ice particle multiplication in cumulus clouds. *Quarterly Journal of the Royal Meteorological Society* **102**, 133–156 (1976).

[45] Phillips, V. T. J. *et al.* Potential impacts from biological aerosols on ensembles of continental clouds simulated numerically. *Biogeosciences* **6**, 987–1014 (2009).

[46] Phillips, V. T. J. *et al.* Improvements to an empirical parameterization of heterogeneous ice nucleation and its comparison with observations. *Journal of the Atmospheric Sciences* **70**, 378–409 (2013).

[47] Phillips, V. T. J., Formenton, M., Bansemer, A., Kudzotsa, I. & Lienert, B. A parameterization of sticking efficiency for collisions of snow and graupel with ice crystals: Theory and comparison with observations. *Journal of the Atmospheric Sciences* **72**, 4885–4902 (2015).

[48] Phillips, V. T. J., Yano, J. I. & Khain, A. Ice multiplication by breakup in ice–ice collisions. part i: Theoretical formulation. *Journal of the Atmospheric Sciences* **74**, 1705–1719 (2017).

[49] Phillips, V. T. J. *et al.* Multiple environmental influences on the lightning of cold-based continental cumulonimbus clouds. part i: Description and validation of model. *Journal of the Atmospheric Sciences* **77**, 3999–4024 (2020).

[50] Leung, L. Arm cloud-aerosol-precipitation experiment (acapex) field campaign report. Tech. Rep., ARM (2016).

[51] Lin, Y. *et al.* Modeling impacts of ice-nucleating particles from marine aerosols on mixed-phase orographic clouds during 2015 acapex field campaign. *Atmospheric Chemistry and Physics* **22**, 6749–6771 (2022).

[52] Lang, T. J. *et al.* The severe thunderstorm electrification and precipitation study. *Bulletin of the American Meteorological Society* **85**, 1107–1126 (2004).

[53] Jensen, M. P. *et al.* The midlatitude continental convective clouds experiment (mc3e). *Bulletin of the American Meteorological Society* **97**, 1667–1686 (2016).

[54] Martin, S. T. *et al.* The green ocean amazon experiment (goamazon2014/5) observes pollution affecting gases, aerosols, clouds, and rainfall over the rain forest. *Bulletin of the American Meteorological Society* **98**, 981–997 (2017).

[55] Romatschke, U. & Houze, R. A. Characteristics of precipitating convective systems accounting for the summer rainfall of tropical and subtropical south america. *Journal of Hydrometeorology* **14**, 25–46 (2013).

[56] Rehbein, A., Ambrizzi, T. & Mechoso, C. R. Mesoscale convective systems over the amazon basin. part i: climatological aspects. *International Journal of Climatology* **38**, 215–229 (2018).

[57] Rehbein, A., Ambrizzi, T., Mechoso, C. R., Espinosa, S. A. I. & Myers, T. A. Mesoscale convective systems over the amazon basin: The goamazon2014/5 program. *International Journal of Climatology* **39**, 5599–5618 (2019).

Supplementary Files

This is a list of supplementary files associated with this preprint. Click to download.

- SIPPartIsppl.pdf